water

MDPI

Article

Imaging of Groundwater Salinity and Seawater Intrusion in Subiya Peninsula, Northern Kuwait, Using Transient Electromagnetics

Firyal Bou-Rabee [1], Pritam Yogeshwar [2,*], Sven Burberg [2], Bülent Tezkan [2], Michael Duane [1] and Ismael M. Ibraheem [2,*]

[1] Department of Earth and Environmental Sciences, Kuwait University, P.O. Box 5969, Safat 13060, Kuwait; firyal.bourabee@ku.edu.kw (F.B.-R.); michael.duane@ku.edu.kw (M.D.)
[2] Institute of Geophysics and Meteorology, University of Cologne, Albertus-Magnus-Platz, 50923 Cologne, Germany; sburberg@smail.uni-koeln.de (S.B.); tezkan@geo.uni-koeln.de (B.T.)
* Correspondence: yogeshwar@geo.uni-koeln.de (P.Y.); ismael.ibraheem@geo.uni-koeln.de (I.M.I.)

Abstract: This study investigates the presence and spatial extent of saline water and seawater intrusion in the Subiya Peninsula, Kuwait, a region designated for the establishment of the new Silk City. We collected transient electromagnetic (TEM) data at 63 stations using a coincident loop setup on a regional, as well as local, scale. The data were analyzed through conventional 1D inversion techniques, including Occam and Levenberg–Marquardt methods, to create detailed resistivity models of the subsurface. Our findings indicate significant variations in groundwater salinity, with increased salinity towards the coast and partly decreasing resistivity with depth, suggesting a transition from brackish to saline water. In the northern region, close to the Abdali farms and Al-Raudhatain freshwater fields, groundwater remains fresher at greater depths, while in the south, saline conditions are encountered, occurring at shallower depths. Local scale analysis reveals potential saltwater intrusion pathways and highlighted geological features such as faults. A thorough understanding of the hydrogeological conditions is crucial, as saltwater injection for oil recovery is common in Kuwait, and may correlate with present-day seismic activity. These insights are critical for the sustainable planning and development of Silk City, emphasizing the necessity for further geophysical studies and borehole data to ensure construction safety and sustainable water supply management. This research provides a foundational understanding of the hydrogeological conditions essential for the successful implementation of the Silk City project and for groundwater management in northern Kuwait.

Keywords: coastal aquifer; saltwater–freshwater interface; aquifer characterization; electromagnetic surveying; groundwater evaluation; Silk City; Kuwait

Academic Editor: Maurizio Polemio

Received: 30 December 2024
Revised: 13 February 2025
Accepted: 21 February 2025
Published: 24 February 2025

Citation: Bou-Rabee, F.; Yogeshwar, P.; Burberg, S.; Tezkan, B.; Duane, M.; Ibraheem, I.M. Imaging of Groundwater Salinity and Seawater Intrusion in Subiya Peninsula, Northern Kuwait, Using Transient Electromagnetics. *Water* **2025**, *17*, 652. https://doi.org/10.3390/w17050652

1. Introduction

Seawater intrusion poses a significant threat to coastal aquifers, endangering freshwater resources essential for drinking water supply, agriculture, and ecological sustainability [1–3]. This phenomenon is primarily driven by over-extraction of groundwater, climate change-induced sea-level rises, and anthropogenic activities, leading to salinization of freshwater reserves [4,5]. In arid and semi-arid regions like Kuwait, where natural freshwater resources are scarce, the issue is particularly critical. The country heavily depends on desalination plants and groundwater extraction from shallow aquifers to meet its growing water demands. However, increasing groundwater exploitation, coupled with saltwater intrusion, poses significant risks to water security and sustainable development.

Kuwait's coastal aquifers are particularly vulnerable to two major sources of subsurface salinization. The first is deep subsurface saltwater injection, a process used in oil recovery that can potentially migrate upward and impact shallow groundwater systems. The second is direct brine infiltration into the shallow subsurface, which can lead to the contamination of water fields, such as those in the northern Al-Raudhatain and Abdali farms. However, saltwater intrusion along Kuwait's coastline has increased due to overexploitation of these aquifers and possible future hazards, such as rising sea levels and saltwater injection activities in Sabriya oilfields [6]. The intrusion not only threatens the availability of potable water, but also compromises agricultural productivity and ecosystem health in coastal areas.

Given the complexity of saltwater intrusion mechanisms, geophysical methods play a crucial role in delineating subsurface hydrogeological conditions. One such technique, loop source transient electromagnetics (TEM), has been widely used in groundwater exploration-related studies, due to its ability to detect resistivity variations in subsurface formations [7–12]. It offers a valuable tool for studying seawater intrusion in coastal aquifers [13–17]. TEM methods are particularly effective for identifying freshwater–seawater interfaces, mapping salinity distribution, and assessing the pathways and progression of saltwater intrusion [18,19]. This information is crucial for understanding the dynamics of saltwater intrusion, predicting its future impacts, and informing effective management and mitigation strategies.

While electric resistivity tomography (ERT) provides high-resolution 2D and 3D imaging of resistivity variations, making it effective for detecting lateral and vertical salinity gradients, it has lower depth penetration, and can be affected by electrode coupling issues in high-salinity environments. Nuclear magnetic resonance (NMR), on the other hand, directly measures water content and porosity, providing valuable hydrogeological information, but its depth penetration is limited, and it is highly sensitive to noise, making it less effective in urban and coastal environments. In contrast, TEM offers deeper penetration and is highly sensitive to conductive layers (ideal for saline groundwater mapping). It enables faster data acquisition compared to ERT, making it more efficient for regional-scale studies. However, TEM has lower near-surface resolution than ERT, and cannot directly measure water content like NMR.

The Subiya Peninsula (Figure 1), located in northern Kuwait, is undergoing rapid transformation due to the Silk City megaproject, one of the country's most ambitious urban development initiatives. Approved in 2010 and scheduled for completion between 2030 and 2035, the Silk City project aims to establish a major economic and residential hub featuring advanced infrastructure, including a 1001-meter-tall skyscraper, an international airport, and a major seaport on Bubiyan Island. This large-scale urban expansion, connected to Kuwait City via the 26-kilometer Jaber Causeway, is expected to drive economic growth and urbanization. However, the sustainability of such extensive development hinges on the availability and quality of groundwater resources, posing significant future socio-economic risks, particularly in light of potential seawater intrusion risks. By mapping affected areas, this study supports sustainable water use, safeguards freshwater reserves, aids urban planning, and informs climate resilience policies, ensuring long-term stability.

Approximately 75% of Kuwait's land is designated for grazing and tourism-related activities, while oil fields occupy 7% and military zones account for 4%. As one of the most water-stressed countries in the world, Kuwait relies heavily on transboundary aquifers to meet its water needs. Kuwait generally experiences low surface runoff due to sparse precipitation and the high permeability of sandy soils. During extreme weather events, such as winter storms, rainfall occurs, but is rapidly absorbed, forming small, saline ephemeral playa lakes. Historically, rainwater infiltration through the Dibdibba Formation of the

Kuwait Group was considered significant in models for the Al-Raudhatain and Umm Al-Aish agricultural zones [20]. However, a study by Al-Hurban et al. [21], which involved excavating six shallow pits in northern Kuwait's drainage basins and analyzing satellite imagery using ArcHydro GIS, revealed limited infiltration capacity and minimal interaction with freshwater lenses at depth. Rainwater that does not accumulate in playas eventually drains seaward.

The water balance in the Subiya Peninsula is highly constrained due to its arid climate. The region experiences low annual precipitation (100 to 120 mm) and high evaporation rates (~2500 mm/year), leading to minimal natural groundwater recharge [22]. Additionally, urban expansion and excessive groundwater extraction have intensified concerns over seawater intrusion into coastal aquifers, threatening water quality and availability [23]. As Subiya transforms from a desert landscape into an urban and industrial hub, large-scale projects such as Silk City and oil extraction activities in Bahra and Sabriya fields further increase water demand and groundwater stress [24]. The Jaber Al-Ahmad Causeway, facilitating regional connectivity, accelerates urbanization and economic growth, adding to water consumption pressures. Given that about 90% of Kuwait's water supply comes from desalination, with groundwater serving mainly agricultural and industrial purposes, addressing water sustainability challenges is critical [25]. Therefore, as Silk City advances, Kuwait must prioritize the expanding desalination capacity, improving water recycling, and protecting coastal aquifers to ensure long-term urban and industrial growth in Subiya.

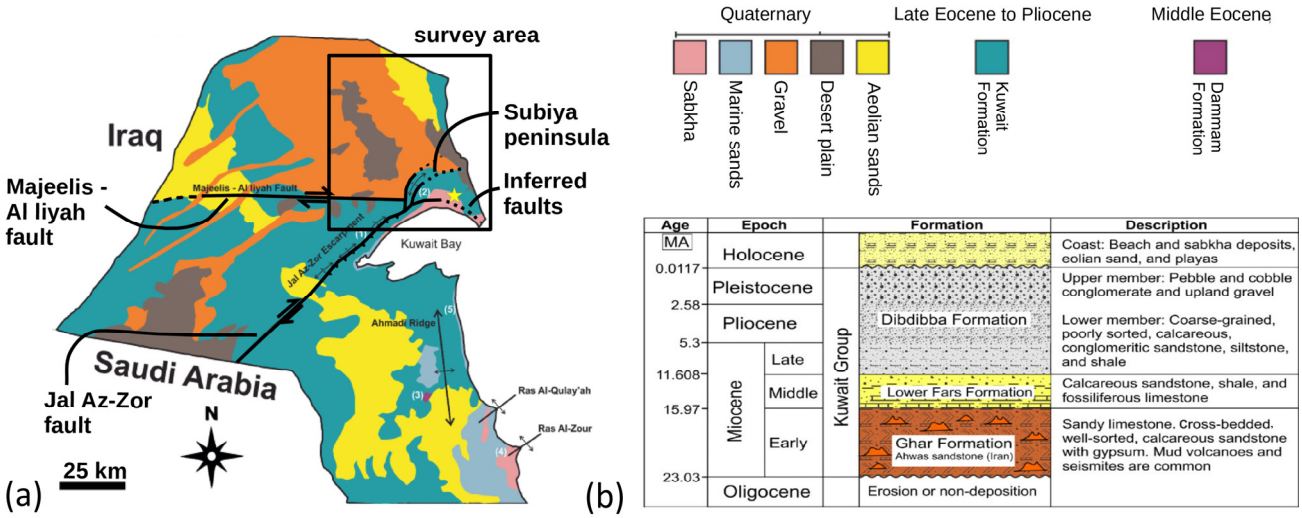

Figure 1. (**a**) A surface geological map of Kuwait illustrating its primary structural features, alongside the distribution and ages of outcrops and sedimentary cover [26]. The focus area of this study, Subiya, is outlined by a black square with coordinates at the lower-left corner at 29°30′50.22″ N, 47°35′43.32″ E, and at the upper-right corner at 30°02′44.28″ N, 48°09′37.26″ E. (**b**) A stratigraphic column of the major geological formations, from the Miocene to Holocene, in the Kuwait Group [27]. The white numbers on the geologic map indicate outcrops: (1) Jal Az-Zor Escarpment, (2) Subiyah, (3) Ahmadi Quarry, (4) Khairan Ridges, and (5) Enjefa Beach.

Despite the recognized threat of saltwater intrusion in Kuwait's coastal aquifers, there remains a notable research gap in assessing its implications for large-scale urban development in arid environments. While previous studies have focused on mapping groundwater salinity in northern Kuwait, comprehensive geophysical investigations specifically addressing the hydrogeological conditions of the Subiya Peninsula remain limited. The increasing reliance on groundwater, coupled with saltwater injection for oil recovery and the anticipated effects of future sea-level rises, underscores the urgent need for a detailed assessment of salinization risks in this region. This study seeks to bridge this critical knowledge gap by

employing TEM surveys to achieve the following objectives: 1. delineate the distribution of saline water within the Subiya Peninsula's aquifers; 2. assess the extent and dynamics of seawater intrusion in the region; and 3. evaluate the potential impact on Silk City's infrastructure and water resource management strategies. By integrating geophysical data with hydrogeological analysis, this research aims to provide scientific insights necessary for developing sustainable groundwater management policies, ensuring long-term water security and infrastructure resilience for Kuwait's future urban expansion.

2. Geological and Hydrogeological Setting

Kuwait largely consists of desert areas. The topography of Kuwait is generally flat, with the surface elevation in the east of the country, near the coast, at 0 m, and in the southwest, at up to 280 m above sea level [28]. The surface is characterized by few elevations, with the Jal Az-Zor and Al-Subyiah elevations in the north and the Al-Ahmadi and Al-Kharian elevations in the south [26]. The most prominent elevation in the country is the Jal Az-Zor Escarpment [29]. The escarpment runs from the southwest to the northeast, up to the survey area in Subiya (cf. Figure 1a). There are various theories about the origin of the Jal Az-Zor elevation [30]. The near-surface structures in Kuwait mainly consist of sedimentary rocks from the early Miocene to the most recent Quaternary period (cf. Figure 1). The Quaternary sediments at the surface are sand deposits containing portions of salt carbonates and limestone. In the northeast of the country, along the coastline of Kuwait Bay, there are tidal flats with Sabkha deposits. The tidal flat sediments consist mainly of alluvial sandstones with a high salt content, and also consist partially of claystones [28]. Beneath the upper deposits lies the so-called Kuwait Group (cf. Figure 1b). This consists of clastic sediments, and can be divided into the following three sections, with increasing depth [31,32]: 1. the Dibdibba Formation (DF), 2. the Lower Fars Formation (LFF), and 3. the Ghar Formation (GF).

The three formations within the Kuwait Group differ in age and sediment composition. A stratigraphic representation of the geological formations within the Kuwait Group is shown in Figure 1b. The DF, from the Miocene to the Pleistocene, is the uppermost layer of the Kuwait Group, and can have a thickness ranging from a few meters to approximately 183 m in the north [33]. The formation consists of sand and gravel with portions of gypsum and clay, and can be divided into two sections [28]. The upper section of the formation primarily comprises coarse gravel, which differs from the deeper layers composed mainly of gravelly sandstone with calcareous carbonates [31,34]. Below the DF lies the LFF, which has a thickness ranging from 60 m in the west to 180 m in the north. This Miocene formation consists of shale, sandstone, and fossiliferous limestone [31,33]. The lowest layer of the Kuwait Group is the GF, from the Oligocene to the early Miocene. The sediments of the GF mainly comprise calcareous sandstone with gypsum components [31].

Kuwait's groundwater resources are limited and vulnerable to over-exploitation, as well as contamination, primarily due to the arid climate, rapid population growth, and extensive urbanization. Annual precipitation occurs predominantly from November to February, with a generally low amount of rainfall [22,35]. However, rainfall patterns vary across the different geographical locations. The groundwater level varies between 0 m along the coast of the Arabian Gulf and Kuwait Bay in the east, and up to 90 m below the surface towards the southwest [33]. Kuwait's groundwater is generally brackish to salty. The exceptions are the freshwater fields 'Al-Raudhatain' and 'Umm Al-Aish' in the north of the country, which represent the only freshwater resources in Kuwait [36]. The Kuwait Group and the underlying Dammam Formation act as groundwater aquifers.

In this work, we focus on understanding the aquifers, and relate the derived subsurface models to the value of 'Total Dissolved Solids' (TDS). TDS describes the number of solids

dissolved in a fluid. In groundwater, mainly salts are dissolved, making the TDS value an indicator of whether the water is fresh or saline. Although the TDS value is usually given in milligrams per liter [mg/L], we use here the unit g/L, due to the generally very high values present in the area.

The LFF acts as an aquitard with lower permeability, separating the Dibdibba and Ghar formations [33,37]. The aquifers in the Kuwait Group show large variations, with TDS values ranging from below 4 g/L for brackish water in the southwest, to values over 100 g/L, indicating hypersaline water, in the northeast near the coast [38]. Below the Kuwait Group is the Dammam Formation, which mainly consists of limestone. It also serves as an aquifer, with TDS values ranging from 2.5 g/L to 200 g/L, increasing from southwest to northeast [33].

In the north lies Kuwait's largest freshwater field, Al-Raudhatain. The TDS values in this area vary from 0.2 g/L to 8 g/L. Water quality decreases with depth, and the freshwater field is surrounded by brackish and saline water, with values sometimes exceeding 14,000 mg/L at the periphery of the area [36]. Freshwater with salinity under 1 g/L can be found in the upper section of the DF, where the system can be distinguished in two aquifers. The upper aquifer has a thickness of 12 to 36 m, and is saturated with freshwater. Below follows an aquifer with a thickness of 11 to 18 m, containing brackish to saline water [36].

Fadlelmawla et al. [38] analyzed the groundwater TDS values in the Kuwait Group. The derived TDS map in Figure 2a is based on borehole data, and provides an overview for the entire country. The survey area presented in this study is marked by a black square. Along the coast of the Arabian Gulf, the TDS values range from 10 to 50 g/L, indicating hypersaline groundwater. Moving westward, the TDS concentration decreases, indicating fresher groundwater. This area includes the farming region of Abdali and the freshwater field of Al-Raudhatain. Al-Senafy et al. [39] analyzed and modeled the groundwater in northern Kuwait by integrating borehole information, as well as TEM measurements. Their study establishes a relationship between the electrical resistivity of groundwater and the TDS value. In our study, we use Archie's empirical law to transform the modeled bulk electrical resistivity into fluid resistivity (ρ_f), and subsequently use the relation proposed by [40] to further transform the ρ_f into TDS values.

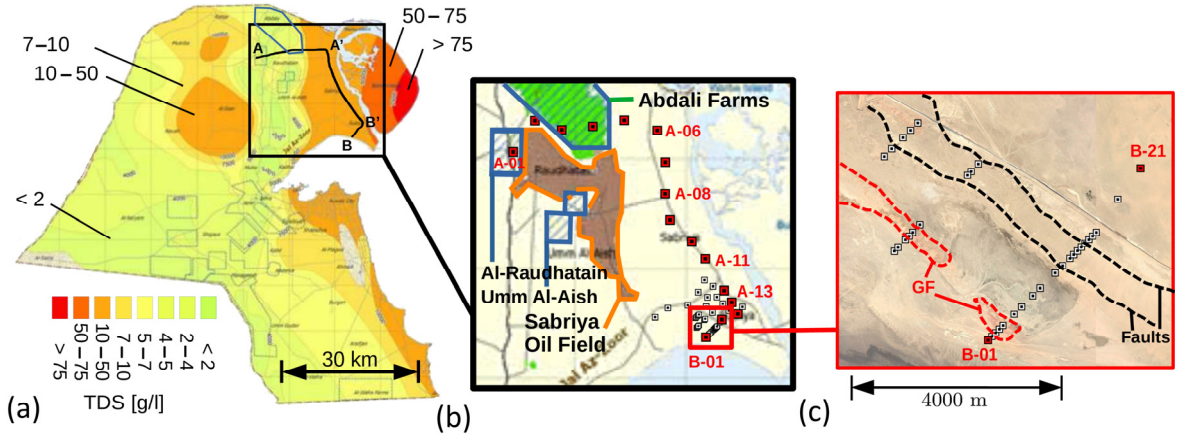

Figure 2. The TEM survey design in Subiya. (**a**) A TDS map, with values in g/L (after [38]). The location of the survey area is marked by a black square. The regional scale profile, with ~70 km length, is indicated by a black line, and is subdivided into three zones: A-A′ (Z1) in the north, A′-B′ (Z2) in the central part, and B′-B (Z3) in the south. (**b**) Soundings along the regional scale profile are marked as red dots. The background image shows the freshwater fields in blue and the Sabriya oil field in brown (after [38]). (**c**) Local scale soundings covering the tidal flats in the south of the Subiya Peninsula. The inferred faults are shown as black dashed lines, and the red GF as a red dashed outline.

3. TEM Survey Design and Data

The TEM method is widely used for imaging subsurface conductive structures [8–11,40,41]. It involves transmitting a current into square loops of insulated wire deployed on the Earth's surface. The transmitter loop's current alternates between time-on and time-off periods, generating a time-varying electromagnetic field, based on Faraday's Law. After the current's switch-off, the primary magnetic field decays. This decay induces eddy currents in the subsurface, which generate a secondary magnetic field recorded by a receiver positioned either at the center or at an off-set distance from the transmitter loop. TEM offers remarkable sensitivity to conductive formations, and enables high-resolution imaging of the subsurface without requiring direct galvanic contact with the ground. The efficiency and application of the TEM method are further detailed in [42,43]. With applications spanning various geological settings, including saline water mapping, TEM has demonstrated its efficiency and versatility in numerous studies worldwide. Despite its strengths, TEM may encounter limitations in highly resistive rock formations or in laterally highly heterogeneous media (e.g., [44]). Nevertheless, its relative simplicity, cost-effectiveness, and ability to probe depths ranging from the surface to depths of a few hundred meters make it a valuable tool for general geological and environmental studies, as well as mineral exploration.

TEM data were gathered utilizing the TEM-FAST portable device, using a coincident loop setup with a single 50 m × 50 m wire loop. The transmitting current was maintained at 4 Amperes, with a recording time ranging between 6 µs and 0.02 s. In total, we covered 63 TEM stations at both local and regional scales, as shown in Figure 2b,c. On the regional scale, 16 soundings, with a varying inter-station spacing between 5 and 10 km, cover a roughly 70 km long profile, from the tidal flats in the south of Subiya towards the freshwater fields around the Abdali farms in the north (cf. Figure 2b). A denser grid of soundings was acquired on a local scale, to image the saltwater intrusion at the coast and around the core area of the planned Silk City construction site (cf. Figure 2c). The station distance is 100 m along the local scale profiles, with a profile distance of roughly 2–3 km. The main profile (B-01–B-21) transects a possible fault zone, with an elevation change of approximately 20 m.

Four exemplary TEM transients are presented as induced voltage and transformed into late-time apparent resistivity ($\rho_{a,\,LT}$) in Figure 3a,b for soundings A-01, A-08, A-13, and B-01. The locations are marked on the map in Figure 2b. A clear change in data characteristics is observed, indicating low resistivity (below 1 Ωm) towards the tidal flats, and higher values towards the freshwater fields around the Abdali farms, with comparably low groundwater TDS values (cf. Figure 2a,b).

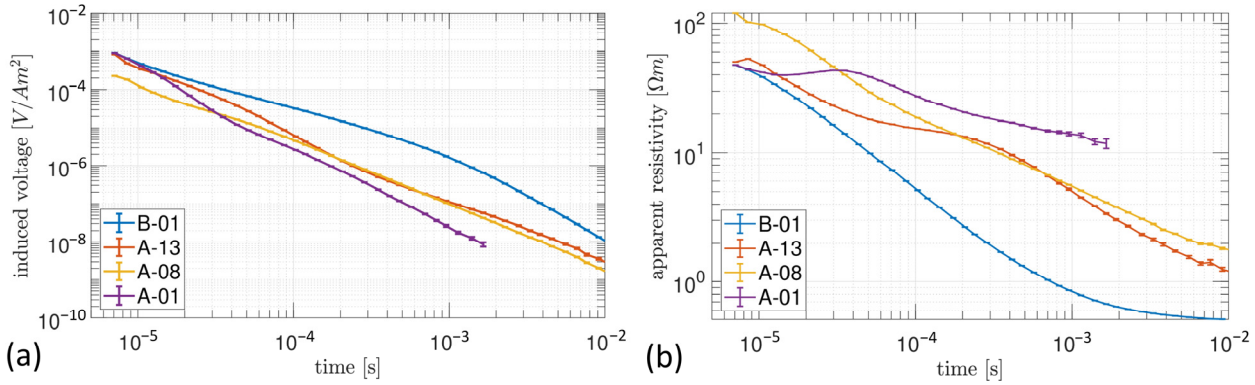

Figure 3. Exemplary TEM data for soundings A-01, A-08, A-13, and B-01. The locations are shown in Figure 2. (**a**) Observed induced voltage decay curves. (**b**) Late-time apparent resistivity curves.

In Figure 4, we present the color-coded late-time apparent resistivity for one transient time, t = 1 × 10^{-3} s. From the late-time apparent resistivity data, a very consistent behavior

along the profile from south to north is observed. The apparent resistivity drops below 1 Ωm on the tidal flats, and surpasses ~10 Ωm towards the Abdali farms, indicating a decrease in subsurface salinity away from the coast. The general trend of the data is consistent with the TDS map in Figure 2a. Note that midway between A′ and B′, we observe a slight increase in $\rho_{a,\,LT}$.

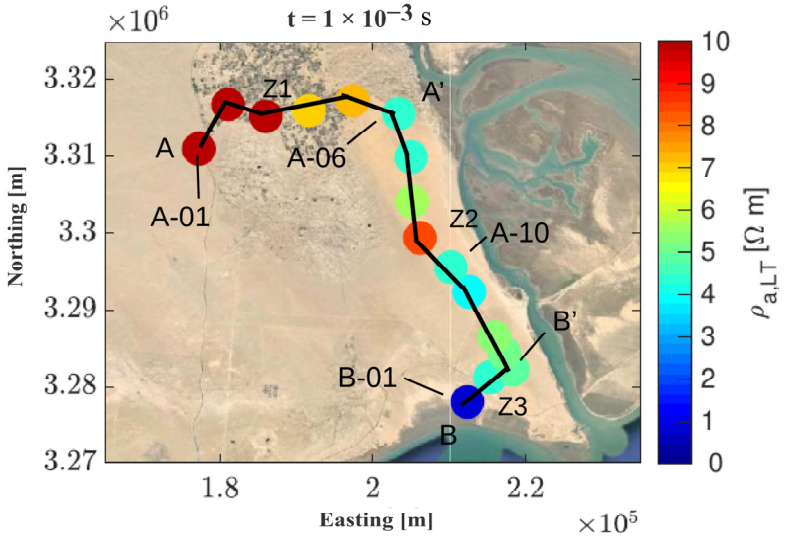

Figure 4. TEM data plotted for one time channel, t = 1 × 10^{-3} s, as late-time apparent resistivity for the regional scale transect. The transect is divided into AA′, A′B′, and B′B.

4. Results and Discussion

Subsequently, 1D inversion of TEM data was carried out using conventional Occam roughness 1 (R1) and roughness 2 (R2), as well as Levenberg–Marquardt (LM) inversion techniques, where Occam R1 applies a first-order smoothness constraint that minimizes changes between consecutive layers, providing a smooth model, while Occam R2 uses a second-order constraint, minimizing the second order difference (curvature) of the models [40]. Both models usually differ at depths where the model parameters are not supported by the data; hence, the divergence of R1 and R2 is often used to estimate the depth of investigation (DOI). Two exemplary 1D models are depicted, together with induced voltage data and model response, in Figure 5. The data are fitted well for both soundings, with chi (χ) values ~1 and reasonable equivalence ranges for the LM models. B-01 is located on the tidal flats, and indicates 2–3 subsurface layers with resistivities below 1 Ωm, already at a depth greater than 10 m below the surface. The lowest resistivity values are observed at 15 m depth, with values around 0.4 Ωm. The DOI estimate is roughly 80 m, using the approach suggested by Spies [45]. Sounding A-01 is located on the Al-Raudhatain freshwater field, and shows much larger resistivity values overall (~6 Ωm at 30 m depth), down to the DOI of roughly 115 m. Note that the divergence of R1/R2 suggests reduced DOI values, with 80 m for A-01 and roughly 50 m for B-01.

4.1. Spatial Distribution of Saline Groundwater

Figure 6 displays the resistivity extracted from the Occam R1 models for the 16 regional TEM stations, at three different depths, on a Google Earth satellite image (top row), on the TDS map from [38] (middle row), and on the topography map from [46] (bottom row). Here, we show the elevations −10 m (left), −30 m (middle), and −60 m (right). These graphics serve to assess the regional salinity in the groundwater, and discuss possible causes for the resistivity variations seen in the presented models, which are possibly related to TDS and altitude.

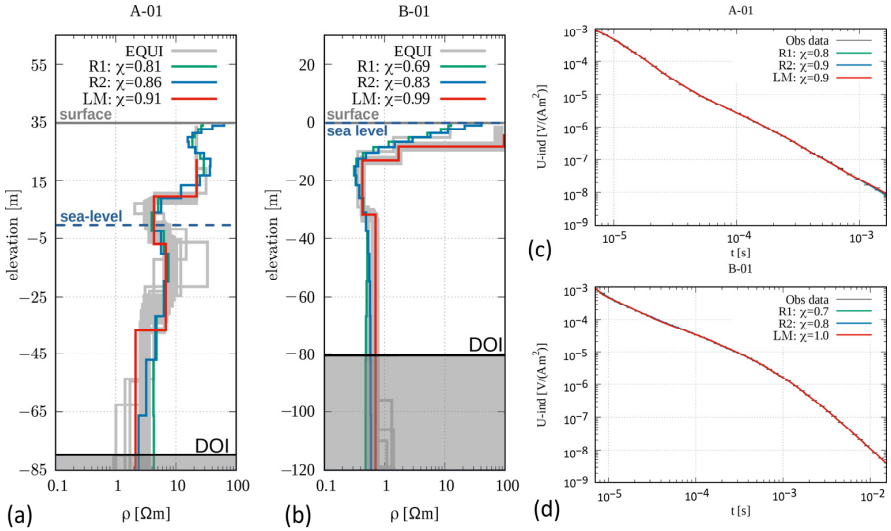

Figure 5. One-dimensional models, together with data and model response, for soundings A-01 (**a**,**c**) and B-01 (**b**,**d**). The data fit chi is displayed in the respective legend. The LM models are marked in red, and the equivalent models (EQUI) in gray. Occam R1/R2 models are marked in green and blue. The DOI, derived based on the approach suggested by Spies [45], is indicated by black lines.

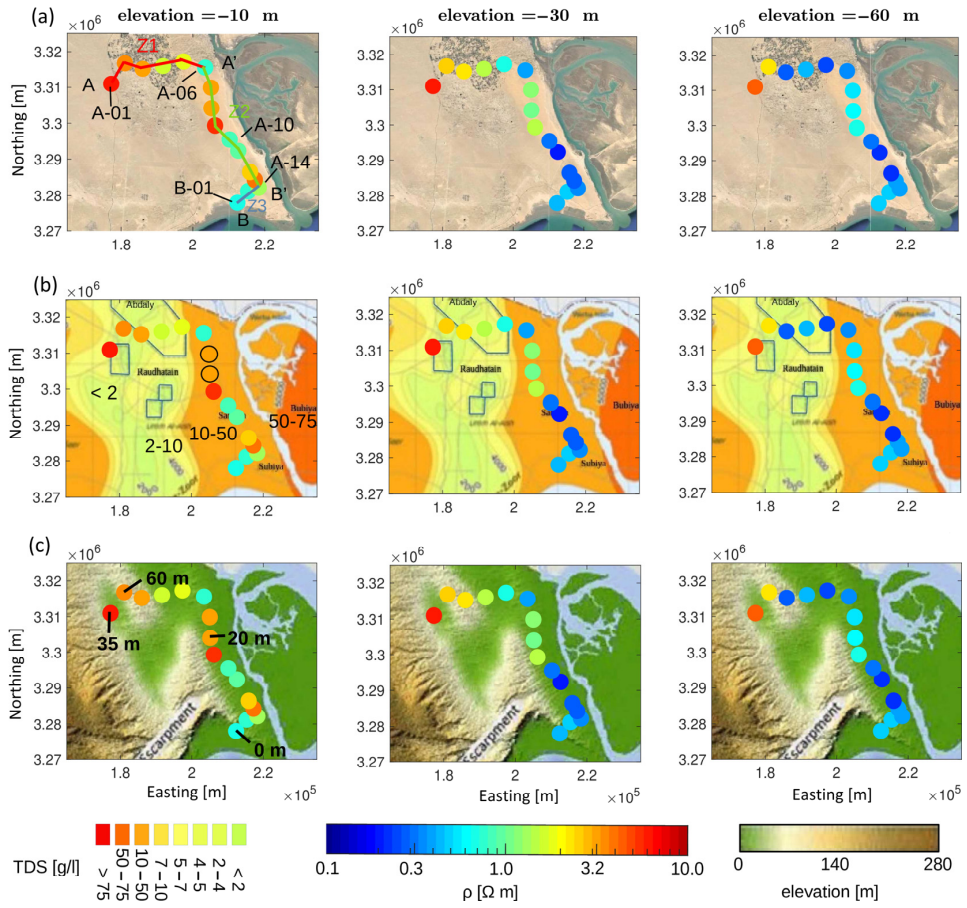

Figure 6. A scatter plot of the modeled subsurface resistivity, depicted on (**a**) the satellite image, together with station/zone labels (top row), (**b**) the TDS map from [38], with values in g/L (middle row), and (**c**) the topography map from [46], with labeled altitude (bottom row). The elevations for the model scatter plots are −10 m, −30 m, and −60 m. The maps are derived from the Occam R1 results.

According to [38], the groundwater level in the northeast of Kuwait ranges from an elevation of 0 m to 10 m. Thus, in the survey area, at all the depths shown in Figure 6, the soil is saturated with groundwater. Note the resistivity variation with increasing depths. At an elevation of −10 m, the resistivities for all soundings are above 1 Ωm, and decrease with depth. For the southern stations (A-10 to B-01), we observe a transition to a more conductive subsurface, with 0.2–0.5 Ωm at an elevation of −30 m. For the northern part of the profile (stations A-1 to A-10), the resistivity remains mainly above 1 Ωm down to an elevation of −30 m. Below this depth, there is a transition to resistivities below 0.8 Ωm. Since the subsurface resistivity decreases with depth, we suggest that the groundwater becomes more saline with increasing depth, indicating a transition from brackish to saline groundwater. The progression from initially fresh to brackish groundwater close to the surface, becoming saline at greater depths, is also reported in [47]. In the southern TEM stations, the transition from brackish to saline water is evident at shallower depths, whereas in the north, this transition occurs at greater depths (see also 1D models in Figure 4 for comparison).

Besides the general behavior of increasing resistivity with depth, a regional pattern is evident at all depths. In zone Z1 (A-A′), the resistivity decreases from west to east, and is higher overall than in the southern zones (Z2, Z3). This trend suggests that groundwater salinity decreases towards the inland areas and increases towards the coastal areas. In zone Z2 (A′-B′), along t'he eastern coast southward, three stations (A-07, A-08, and A-09) stand out with higher resistivity. At these stations, the salinity is lowered, possibly due to a freshwater recharge from terrain elevations in the west (Figure 6, bottom row). The resistivity increases towards Abdali, which aligns well with the decrease in TDS values of the groundwater. Noteworthy is station A-01, located in the Al-Raudhatain freshwater field. As visible in Figure 6 (bottom row), Al-Raudhatain is situated in a valley, and surrounded by 12 dry riverbeds that are flooded during heavy rains, ensuring natural groundwater recharge [33,36]. In Al-Raudhatain, the TDS values range from 0.2 to 8 g/L. Similarly, the TDS values are significantly lower in Abdali compared to zone Z2 along the profile. The fresher groundwater at Al-Raudhatain is confirmed by higher resistivities at all depths for soundings A-01 and A-02. For the Abdali soundings (A-03, A-04, and A-05), the groundwater remains fresher down to an elevation of −40 m. Below this, there is a transition to saline groundwater, with resistivities of roughly 0.3 Ωm.

4.2. Regional Scale Interpretation

The 1D Occam R1 models are stitched together as quasi-2D sections along the regional profile A-B (cf. Figure 7). We use a linear interpolation between the soundings. The profile is subdivided into three distinct sections (Z1 to Z3, cf. Figure 7). We observe three distinct layers that are interpreted in terms of geological and hydrogeological knowledge, namely Holocene deposits (HD) and groundwater aquifers (AQ1 and AQ2).

The northern DF, which is the uppermost geological formation of the Kuwait Group, has a thickness of up to 183 m [33]. Due to a DOI of maximum ~100 m, TEM resolves only information about the DF as the primary aquifer beneath the surface deposits.

- HD: The surface layer consists of Holocene sand and gravel deposits, with resistivities ranging from 20 Ωm to ~300 Ωm. Values vary due to locally different soil compositions and water saturation. This layer may already be partially saturated due to rain infiltration. The depth to the first aquifer ranges from a few meters, to 25 m in elevated areas.
- AQ1: This refers to the upper DF, serving as the shallow aquifer, and primarily consists of sand- and gravel-rich sediments. The transition between HD and AQ1 is as low as z = 0 m at location B-01, and reaches up to an elevation of 41 m at A-01 due to the

elevated topography. The resistivity ranges from 2 to 10 Ωm. Thus, the upper section of the DF is likely saturated with brackish water.

– AQ2: below AQ1, the resistivity decreases to between ~0.2 and 1.0 Ωm. The transition occurs at an elevation of 5 m to roughly −50 m (A-03), caused by increasing salinity. The lower DF differs in structure, being coarser and mainly composed of cemented sandstone. As seen in the 1D stitched models (Figure 7), there is a noticeable resistivity increase in zone Z2 between stations A-07 to A-09 down to roughly −40 m elevation, extending even further downwards. This possibly indicates freshwater recharge from the western elevated terrain (Figure 6). However, with values between 0.7 and 1.0 Ωm, the groundwater is still likely to be saline. In zone Z1, a lateral transition from saline to brackish groundwater occurs between A-03 and A-02, with resistivities varying from 0.2 Ωm to 4.5 Ωm at an elevation of −75 m. Conclusively, the groundwater is likely to be brackish near the freshwater field of Al-Raudhatain.

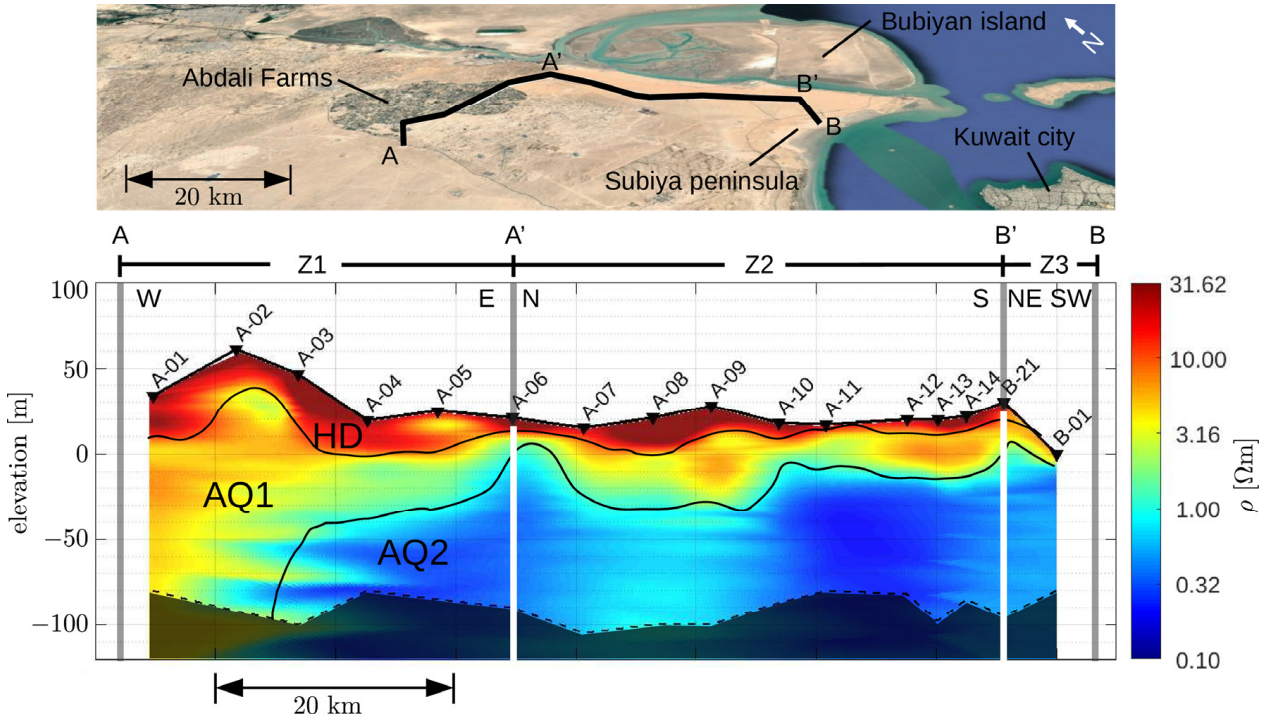

Figure 7. The stitched and interpolated 1D resistivity section derived from the Occam R1 results. For improved visualization, the models are linearly interpolated along the profile. The black lines indicate the transitions between the different layers in the DF. The formations are labeled. The vertical gray/white lines separate the zones Z1, Z2, and Z3 (cf. Figure 6). Note that Z3 is oriented NE–SW. The DOI is marked as the black shaded area.

4.3. Local Scale Interpretation

Figure 8a depicts the late-time apparent resistivity at t = 1 × 10^{-3} s as a scatter plot, and (c) depicts the stitched 1D models obtained in the southern zone Z3. The spatial data pattern indicates a significant resistivity decrease towards the coastline. We observe a few rather distinct zones in the model, marked as Res1, F1, IZ, C1 and C2. The surface layer Res1 shows resistivities larger than 5 Ωm, with a thickness ranging from a few meters in the south, to roughly 40 m towards location B-21. Note that the resistivity decreases between B-11 and B-18, which coincides with the visible known fault at the surface (F1). It is likely that due to the higher porosity around the fault zone, there is either an upwelling of saline water or higher freshwater recharge. Towards the north, we observe an interface zone (IZ) below the resistive zone Res1. From south to north (B-01–B-21), a more conductive

layer (C1) appears, which may indicate a seawater intrusion pathway. The shape of the top of the seawater intrusion can be partly explained by the Ghyben–Herzberg relation, which describes the relationship between freshwater and saltwater in coastal aquifers, estimating that for every meter of freshwater above sea level, there is approximately 40 m of freshwater below sea level before reaching saline water [48]. Assuming the saltwater interface to be at an elevation of −40 m at sounding B-19, the freshwater level would be at an elevation of roughly 1 m. Below C1, the resistivity slightly increases to ~0.6 Ωm, indicating a more compact formation (C2), being shallowest right below the visible outcrops of the red GF (cf. Figure 8b,c). A unique interpretation is difficult, due to the absence of borehole information. However, a relation between the possible fluid pathways, the fault zones, and the known geological formations in this area is visually evident. This may have significant implications for the planning of the 'Silk City' regarding not only construction safety, but also water supply. Further geophysical studies could shed light on this matter.

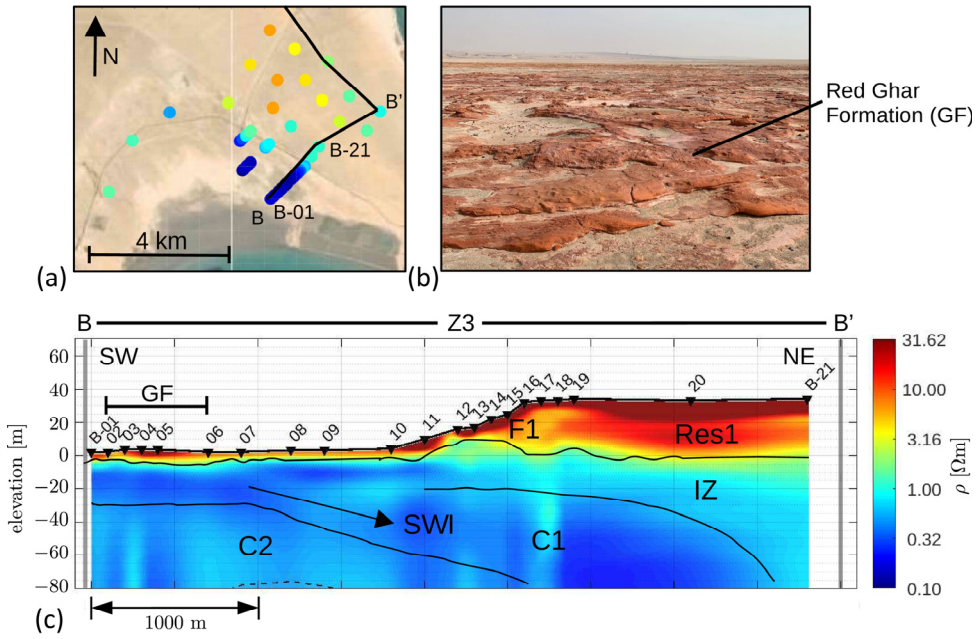

Figure 8. (**a**) A color-coded map of apparent resistivity late-time data for t = 1 ms. (**b**) An image of the outcrop of the red GF. (**c**) A stitched and interpolated 1D resistivity section derived from the Occam R1 results for the local scale transect (B-B') at the Subiya coast. The inferred formations are labeled. Note that Z3 is oriented from SW to NE.

4.4. Transformation of Models to Fluid Resistivity and TDS

Based on Archie's formula, Al-Senafy et al. [39] derived a relationship between TDS values, water, and soil electrical resistivity for northern Kuwait, by the incorporation of TEM data, inferred borehole formation data, and well TDS:

$$\rho_f = 1/(1.3657 \cdot \mathrm{TDS} + 146.82) \cdot 10^{-4} \quad (1)$$

Table 1 shows the various salinity categories and their corresponding TDS values [49]. Using Equation (1), the fluid resistivity values for each salinity category (fresh, brackish, and saline) were calculated.

Table 1. The different salinity categories with their corresponding TDS and fluid resistivity values.

Salinity Category	TDS (g/L)	Water ρ_f (Ωm)
Fresh	0–1	>6.61
Brackish	1–10	0.72–6.61
Saline	>10	<0.72

Figure 9a depicts the TEM sounding A-01, which is located nearby the Al-Raudhatain freshwater field. First, we calculated ρ_f from the model resistivities using Archie's equation ($\rho_f = \rho_{model}/F$), with the formation factors (F) proposed by Al-Senafy et al. [39], and plotted them versus the depth, as shown in Figure 9b. With Equation (1), proposed by Al-Senafy et al. [39], we subsequently solved for the TDS value of the fluid, and plotted it versus depth, as shown in Figure 9c. Note that for near-surface sands with higher porosity, a formation factor of F = 3.1–3.5 is specified, while for deeper areas, the formation factor for cemented sandstone can be up to F = 21. For the lower formation factors (e.g., F = 3.1, sand and gravel), the TDS values are in the brackish range, between 2 and 7 g/L. For higher formation factors (e.g., F = 21, sandstone), the TDS can also be saline, with a TDS value over 10 g/L. According to [36], there are two aquifers in the DF at Al-Raudhatain. The upper aquifer (AQ1) contains fresh groundwater, while the lower aquifer (AQ2) is saturated with brackish to saline water, and with increasing depth, there is cemented sandstone, with a higher formation factor, that is saturated with saltwater. Note that the formation factors are based on estimates provided by Al-Senafy et al. [39], which are derived from distinct borehole analysis. For a more accurate interpretation, data from boreholes along the survey profile line A-B are required, and could allow for more accurate information about the formation parameters necessary for using Archie's empirical equation.

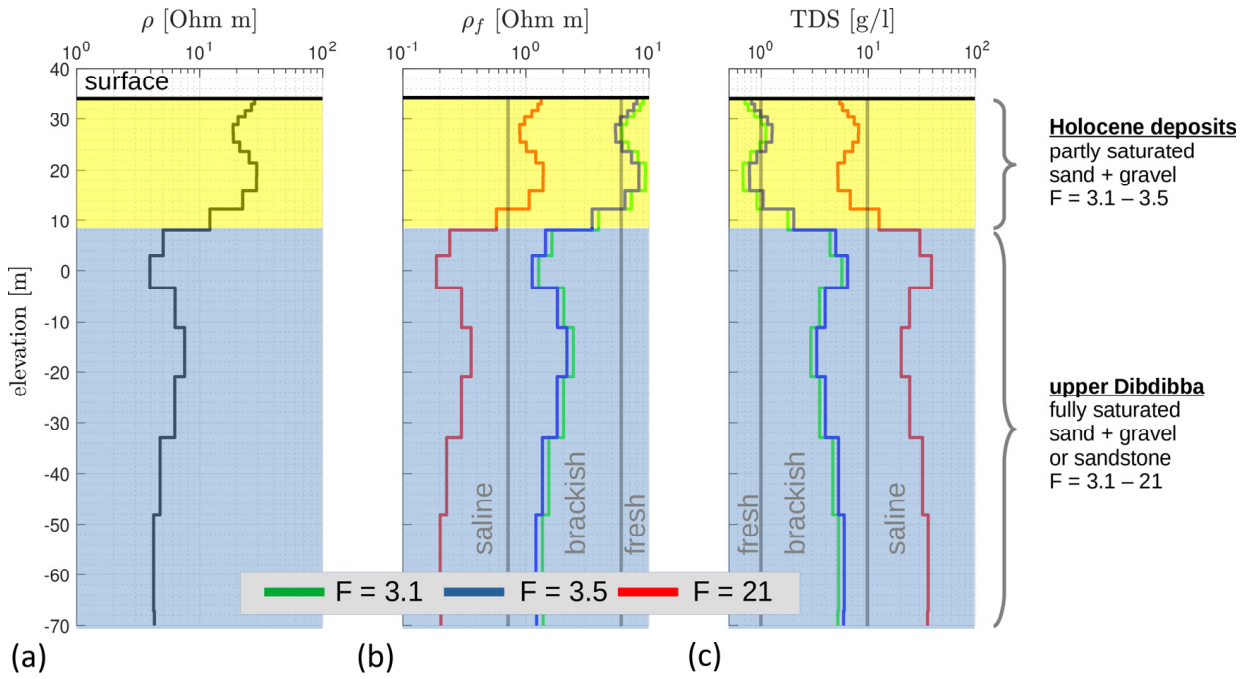

Figure 9. (**a**) One-dimensional models for sounding A-01, (**b**) the derived fluid resistivity ρ_f [Ωm], and (**c**) the TDS value [g/L] of the fluid. The values of ρ_f and TDS are shown for formation factors F = 3.1, 3.5, and 21. The yellow area indicates partially saturated soil; the blue area indicates fully saturated soil. Note that the DOI is at roughly −80 m elevation, and, therefore, is not plotted (see the DOI in Figure 5a).

4.5. Geophysical Insights for Sustainable Engineering in Silk City

The study's findings regarding groundwater salinity and seawater intrusion in the Subiya Peninsula provide critical insights for engineering construction and urban development in the Silk City project area. Variations in groundwater conditions, such as high salinity in coastal zones and fresher water in northern regions like the Al-Raudhatain and Abdali farms, directly impact construction stability and material durability. Saline water poses a corrosion risk to infrastructure, necessitating corrosion-resistant designs or avoidance of high-salinity areas. The identified fault features further highlight construction safety concerns, guiding site selection and mitigation strategies. Additionally, the correlation between terrain elevation and freshwater recharge zones informs sustainable water resource management, ensuring reliable freshwater supply for urban and agricultural needs. Data on water content and bulk resistivity also offer valuable insights into subsurface porosity, which are essential for assessing soil properties and infrastructure design.

However, this study is only a preliminary step; large-scale projects like Silk City require comprehensive geophysical surveys and deep borehole data to refine interpretations and ensure long-term safety. Government agencies should prioritize providing baseline geophysical data, and support further investigations to address risks such as saltwater intrusion, groundwater depletion, and potential seismic impacts from saltwater injection practices. By integrating these findings into urban planning frameworks, the research will enhance construction resilience, support sustainable resource allocation, and mitigate risks, ultimately ensuring the success of multi-billion-dollar developments in the region.

5. Conclusions

This study concludes that the Subiya Peninsula exhibits significant variations in groundwater salinity, which are critical for the proposed Silk City development in terms of sustainable freshwater supply, but also with respect to agricultural progress at the Abdali farms. Regional- and local-scale surveys, well-validated with TDS salinity maps, reveal a clear spatial trend: coastal areas exhibit higher salinity, while northern regions towards the Al-Raudhatain and Abdali farms maintain fresher groundwater at greater depths. The spatial trend correlates with the terrain elevation, possibly indicating zones of increased freshwater recharge. Although Al-Raudhatain shows the least subsurface conductivities, fresh-to brackish water occurs predominantly only in the Holocene deposits, whereas water in the upper DF is likely to be brackish, or even saline. In contrast, southern regions experience saline conditions at shallower depths, likely due to saltwater intrusion pathways influenced possibly by faults. These also indicate increased freshwater recharge or upwelling of fluids. The saltwater intrusion pathway aligns roughly with the Ghyben–Herzberg relation. Towards the coast, a subsurface resistivity pattern below the GF is slightly visible. However, no unique interpretation can be made without deep borehole data to better understand formation factors.

Our findings confirm the need for more spatial geophysical data on a regional scale and detailed hydrogeological assessments, in order to improve regional interpretation and ensure construction safety and sustainable water resource management in the Silk City project area. This deeper understanding of saltwater intrusion pathways provides actionable insights into mitigating salinization risks for planned developments such as Silk City. Specifically, integrating geophysical findings into urban planning frameworks ensures construction resilience and sustainable resource allocation. Implementing a monitoring concept at the Abdali farms and Al-Raudhatain freshwater fields is highly advised to track changes over time, especially to monitor whether the saltwater interface moves towards the freshwater fields due to extensive groundwater abstraction. Further groundwater depletion poses a significant threat to the agricultural production at Abdali and the food supply for

the Kuwait population. Saltwater injection for enhanced oil recovery is a common practice in northern Kuwait. Although the correlation between injection and recent shallow seismic movements (less than 2 km depth) is not yet quantified, further investigation is needed.

By integrating these insights into engineering construction practices and complementing them with further detailed studies, the research enhances its application value, offering actionable data to mitigate risks, optimize resource use, and ensure the long-term resilience and sustainability of the Silk City project and surrounding agricultural areas. While TEM alone provides a strong basis for salinity assessment, future studies could integrate ERT for improved near-surface resolution, and NMR for improved hydrogeological characterization. This combined approach would enhance the accuracy of salinity detection and provide a more comprehensive understanding of groundwater conditions.

Author Contributions: Conceptualization, F.B.-R., P.Y., B.T., M.D. and I.M.I.; data curation, P.Y. and I.M.I.; formal analysis, P.Y., S.B. and I.M.I.; funding acquisition, F.B.-R. and B.T.; investigation, P.Y., S.B. and M.D.; methodology, F.B.-R., P.Y., S.B., B.T., M.D. and I.M.I.; project administration, F.B.-R. and B.T.; resources, F.B.-R., P.Y., B.T. and M.D.; software, P.Y. and S.B.; supervision, P.Y., B.T. and I.M.I.; validation, P.Y., B.T. and I.M.I.; visualization, P.Y., S.B. and I.M.I.; writing—original draft, P.Y., S.B. and I.M.I.; writing—review and editing, P.Y. and I.M.I. All authors have read and agreed to the published version of the manuscript.

Funding: This research received no external funding.

Data Availability Statement: The raw data supporting the conclusions of this article will be made available by the authors on request.

Acknowledgments: The authors express their gratitude to the editor and the five anonymous reviewers for their valuable and constructive feedback.

Conflicts of Interest: The authors declare no conflicts of interest.

References

1. Akhtar, J.; Sana, A.; Tauseef, S.M. Review: Assessment and modeling of seawater intrusion in coastal aquifers of the Arabian Peninsula. *Hydrogeol. J.* **2023**, *31*, 1121–1145. [CrossRef]
2. BinMakhashen, G.M.; Benaafi, M. Predicting seawater intrusion in coastal areas using machine learning: A case study of arid coastal aquifers, Saudi Arabia. *Groundw. Sustain. Dev.* **2024**, *26*, 101300. [CrossRef]
3. Hossain, I.; Reza, S.; Shafiuzzaman, S.M.; Sultan-Ul-Islam, M. Effect of seawater intrusion on water quality of coastal aquifer of Bagerhat district, Bangladesh. *Int. J. Energy Water Res.* **2024**, *8*, 123–140. [CrossRef]
4. Lyra, A.; Loukas, A.; Sidiropoulos, P.; Mylopoulos, N. Climatic Modeling of Seawater Intrusion in Coastal Aquifers: Understanding the Climate Change Impacts. *Hydrology* **2024**, *11*, 49. [CrossRef]
5. Moorthy, P.; Sundaramoorthy, S.; Roy, P.D.; Usha, T.; Dash, S.K.; Gowrappan, M.; Chokklingam, L. Evaluation of spatial and temporal dynamics of seawater intrusion in coastal aquifers of southeast India: Insights from hydrochemical facies analysis. *Environ. Monit. Assess.* **2024**, *196*, 179. [CrossRef]
6. Kuwait Oil Company. Lessons Learned from Two Decades of Water Injection in North Kuwait, Report. 2018. Available online: https://www.kockw.com/sites/EN/EMagazine/Pages/Technology/Lessons-Learned-from-Two-Decades-of-Water-Injection-in-North-Kuwait-.aspx (accessed on 10 April 2024).
7. Ibraheem, I.M. Geophysical Potential Field Studies for Developmental Purposes at El-Nubariya—Wadi El-Natrun Area, West Nile Delta, Egypt. Ph.D. Thesis, Mansoura University, Mansoura, Egypt, 2009; pp. 155–171.
8. Danielsen, J.E.; Auken, E.; Jørgensen, F.; Søndergaard, V.; Sørensen, K.I. The application of the transient electromagnetic method in hydrogeophysical surveys. *J. Appl. Geophys.* **2003**, *53*, 181–198. [CrossRef]
9. Auken, E.; Jørgensen, F.; Sørensen, K.I. Large-scale TEM investigation for groundwater. *Explor. Geophys.* **2003**, *34*, 188–194. [CrossRef]
10. Lévesque, Y.; Walter, J.; Chesnaux, R. Transient Electromagnetic (TEM) Surveys as a First Approach for Characterizing a Regional Aquifer: The Case of the Saint-Narcisse Moraine, Quebec, Canada. *Geosciences* **2021**, *11*, 415. [CrossRef]

11. Ibraheem, I.M.; Othman, A.; Ghazala, H. Pliocene Aquifer Characterization Using TEM and VES Geophysical Techniques: Case Study at the Area to the East of Wadi El-Natrun City, West Nile Delta, Egypt. In *Sustainability of Groundwater in the Nile Valley, Egypt*; Negm, A.M., El-Rawy, M., Eds.; Earth and Environmental Sciences Library; Springer: Cham, Switzerland, 2022; pp. 235–266. [CrossRef]
12. Zamora-Luria, J.C.; McLachlan, P.; Maurya, P.K.; Liu, L.; Grombacher, D.; Christiansen, A.V. A feasibility study on time-lapse transient electromagnetics for monitoring groundwater dynamics. *Geophysics* **2023**, *88*, E135–E146. [CrossRef]
13. El-Kaliouby, H. Mapping Sea water intrusion in coastal area using time-domain electromagnetic method with different loop dimensions. *J. Appl. Geophys.* **2020**, *175*, 103963. [CrossRef]
14. Kalisperi, D.; Kouli, M.; Vallianatos, F.; Soupios, P.; Kershaw, S.; Lydakis-Simantiris, N. A Transient ElectroMagnetic (TEM) Method Survey in North-Central Coast of Crete, Greece: Evidence of Seawater Intrusion. *Geosciences* **2018**, *8*, 107. [CrossRef]
15. Ez-zaouy, Y.; Bouchaou, L.; Schreiber, H.; Montcoudiol, N.; Kalberkamp, U.; Danni, S.O.; Tauab, A.; Abourrig, F.; Hssaisoune, M. Combined geophysical methods to investigate seawater intrusion in the Souss-Massa coastal area, Morocco. *Groundw. Sustain. Dev.* **2023**, *21*, 100915. [CrossRef]
16. Wang, L.; Dai, Y.; Liu, W.; Zhou, S.; Long, X.; Xi, Z.; Xue, J.; Wang, W. Deep Learning Transient Electromagnetic Inversion for Seawater Intrusion. *J. Geophys. Eng.* **2024**, *21*, 1810–1821. [CrossRef]
17. Zhu, Z.; Shan, Z.; Pang, Y.; Wang, W.; Chen, M.; Li, G.; Sun, H.; Revil, A. The transient electromagnetic (TEM) method reveals the role of tectonic faults in seawater intrusion at Zhoushan islands (Hangzhou Bay, China). *Eng. Geol.* **2024**, *330*, 107425. [CrossRef]
18. AbuRajab, J.; El-Kaliouby, H.; Al-Tarazi, E.; AlAmoush, H. Multiscale geoelectrical characteristics of seawater intrusion along the eastern coast of the Gulf of Aqaba, Jordan. *J. Appl. Geophys.* **2023**, *208*, 104868. [CrossRef]
19. El-Kaliouby, H.; Abdallah, O. Application of time-domain electromagnetic method in mapping saltwater intrusion of a coastal alluvial aquifer, North Oman. *J. Appl. Geophys.* **2015**, *115*, 59–64. [CrossRef]
20. Al-Ruwaih, F.; Hadi, K. Water quality trends and management of fresh groundwater at Al-Rawdhatain, Kuwait. *Eur. J. Sci. Res.* **2005**, *9*, 40–64.
21. Al-Hurban, A.; Al-Ruwaih, F.; Al-Dughairi, A. Quantitative Geomorphological and Hydromorphometric Analysis of Drainage Basins of As Sabriyah (Kuwait) Using GIS Techniques. *J. Geogr. Inf. Syst.* **2021**, *13*, 166–193. [CrossRef]
22. Sabarathinam, C.; Bhandary, H.; Ali, A. Strategies to characterize the geochemical interrelationship between coastal saline groundwater and seawater. *Environ. Earth Sci.* **2021**, *80*, 642. [CrossRef]
23. Bhandary, H.; Sabarathinam, C.; Al-Khalid, A. Occurrence of hypersaline groundwater along the coastal aquifers of Kuwait. *Desalination* **2018**, *436*, 15–27. [CrossRef]
24. Kamal, H.J.; Thomas, M.; Abdulhadi, A. Perspectives of Geography, Environment, and Physiography of Kuwait. In *Terrestrial Environment and Ecosystems of Kuwait*; Suleiman, M.K., Shahid, S.A., Eds.; Springer: Cham, Switzerland, 2024; pp. 21–55. [CrossRef]
25. Hadi, K. Current Status, Challenges, and Future Management Strategies for Water Resources of Kuwait. In *Terrestrial Environment and Ecosystems of Kuwait*; Suleiman, M.K., Shahid, S.A., Eds.; Springer: Cham, Switzerland, 2024; pp. 141–169. [CrossRef]
26. Al-Refaei, Y.; Najem, A.; Amer, A.; Al-Qattan, F. Surface Geology of Kuwait. In *The Geology of Kuwait. Regional Geology Reviews*; Abdel-aal, A.K., Al-Awadhi, J.M., Al-Dousari, A., Eds.; Springer: Cham, Switzerland, 2023; pp. 1–25. [CrossRef]
27. Al-Helal, A.; AlRefai, Y.; AlKandari, A.; Abdullah, M. Subsurface Stratigraphy of Kuwait. In *The Geology of Kuwait. Regional Geology Reviews*; Abdel-aal, A.K., Al-Awadhi, J.M., Al-Dousari, A., Eds.; Springer: Cham, Switzerland, 2023. [CrossRef]
28. Milton, D.I. *Geology of the Arabian Peninsula; Kuwait*; Professional Paper; US Geological Survey: Reston, VA, USA, 1967; pp. F1–F7.
29. Amer, A.; Al-Hajeri, M.; Najem, A.; Al-Qattan, F. Facies architecture of Lower Fars Formation at Jal Az-Zor escarpment, Kuwait. *Arab. J. Geosci.* **2019**, *12*, 502. [CrossRef]
30. Al-Sarawi, M. The origin of the Jal-Az Zor escarpment. *J. Univ. Kuwait* **1982**, *9*, 151–162.
31. Duane, M.J.; Reinink-Smith, L.; Eastoe, C.; Al-Mishwat, A.T. Mud volcanoes and evaporite seismites in a tidal flat of northern Kuwait—Implications for fluid flow in sabkhas of the Persian (Arabian) Gulf. *Geo-Mar. Lett.* **2015**, *35*, 237–246. [CrossRef]
32. Owen, R.M.; Naser, S.N. Stratigraphy of the Kuwait-Basrah area. Habitat of Oil. *Am. Assoc. Pet. Geol.* **1958**, *42*, 1252–1278.
33. Misak, R.; Hussain, W. Groundwater in Kuwait. In *The Geology of Kuwait. Regional Geology Reviews*; Abdel-aal, A.K., Al-Awadhi, J.M., Al-Dousari, A., Eds.; Springer: Cham, Switzerland, 2023; pp. 199–214.
34. Al-Sulaimi, J.; Mukhopadhyay, A. An overview of the surface and near-surface geology, geomorphology and natural re-sources of Kuwait. *Earth-Sci. Rev.* **2000**, *50*, 227–267. [CrossRef]
35. Alkandari, A.J. Climate and Climate Change Aspects of Kuwait. In *Terrestrial Environment and Ecosystems of Kuwait*; Suleiman, M.K., Shahid, S.A., Eds.; Springer: Cham, Switzerland, 2023; pp. 57–91. [CrossRef]
36. Hadi, K.M.; Al-Ruwaih, F.M. Geochemical evolution of the fresh groundwater in Kuwait desert. *Emir. J. Eng. Res.* **2008**, *13*, 37–45.
37. Fadlelmawla, A.; Al-Otaibi, M. Analysis of the water resources status in Kuwait. *Water Resour. Manag.* **2005**, *19*, 555–570. [CrossRef]

38. Fadlelmawla, A.A.; Fayad, M.; El-Gamily, H.; Rashid, T.; Mukhopadhyay, A.; Kotwicki, V. A Land Surface Zoning Approach Based on Three-Component Risk Criteria for Groundwater Quality Protection. *Water Resour. Manag.* **2011**, *25*, 1677–1697. [CrossRef]
39. Al-Senafy, M.; Fadlelmawla, A.; Bhandary, H.; Al-Khalid, A.; Rashid, T.; Al-Fahad, K.; Al-Salma, B. Assessment of Usable Groundwater Reserve in Northern Kuwait. *Int. J. Sci. Eng. Res.* **2013**, *4*, 2427–2436.
40. Yogeshwar, P.; Küpper, M.; Tezkan, B.; Rath, V.; Kiyan, D.; Byrdina, S.; Cruz, J.; Andrade, C.; Viveiros, F. Innovative boat-towed transient electromagnetics—Investigation of the Furnas volcanic lake hydrothermal system, Azores. *Geophysics* **2020**, *85*, E41–E56. [CrossRef]
41. Ibraheem, I.M.; Yogeshwar, P.; Bergers, R.; Tezkan, B. Joint interpretation of magnetic, transient electromagnetic, and electric resistivity tomography data for landfill characterization and contamination detection. *Sci. Rep.* **2024**, *14*, 30616. [CrossRef] [PubMed]
42. Kaufman, A.A.; Keller, G.V. *Frequency and Transient Soundings*; Elsevier: Amsterdam, The Netherlands, 1983.
43. Nabighian, M.N.; Macnae, J.C. Time Domain Electromagnetic Prospecting Methods. In *Investigations in Geophysics No 3*; Nabighian, M.N., Ed.; Electromagnetic Methods in Applied Geophysics; Society of Exploration Geophysicists: Tulsa, OK, USA, 1991; pp. 427–514. [CrossRef]
44. Yogeshwar, P.; Tezkan, B. Analysing two-dimensional effects in central loop transient electromagnetic sounding data using a semi-synthetic tipper approach. *Geophys. Prospect.* **2018**, *66*, 444–456. [CrossRef]
45. Spies, B.R. Depth of Investigation in Electromagnetic Sounding Methods. *Geophysics* **1989**, *54*, 872–888. [CrossRef]
46. Naqi, M.; Amer, A. Abdel-aal, A.K., Al-Awadhi, J.M., Al-Dousari, A., Eds.; Structures and Tectonics of Kuwait. In *The Geology of Kuwait. Regional Geology Reviews*; Springer: Cham, Switzerland, 2023; pp. 99–115. [CrossRef]
47. Hadi, K.; Saravana Kumar, U.; Al-Senafy, M.; Bhandary, H. Environmental isotope systematics of the groundwater system of southern Kuwait. *Environ. Earth Sci.* **2016**, *75*, 1096. [CrossRef]
48. Bear, J. *Hydraulics of Groundwater*; McGraw-Hill Series in Water Resources and Environmental Engineering; McGraw-Hill: New York, NY, USA, 1979; pp. 384–385.
49. Aliewi, A.; Al-Kandari, J.; Al-Khalid, A.; Bhandary, H.; Al-Qallaf, H. Modelling the effect of high level of total dissolved solids (TDS) for the sustainable utilization of brackish groundwater from saline aquifers in Kuwait. *Environ. Dev. Sustain.* **2021**, *23*, 2204–2223. [CrossRef]